Mechanical properties of granular media, including snow, investigated by a low-frequency forced torsion pendulum

G. D'Anna

Institut de Génie Atomique, Ecole Polytechnique Fédérale de Lausanne, CH-1015 Lausanne, Switzerland

The oscillating probe of a low-frequency forced torsion pendulum is immersed into various granular media, such as natural sand, glass beads, and granular snow. A first layer of particles is in general solidly bound to the probe surface. The principle of operation and a rheological model are presented. The measured dynamic moduli systematically show a peak of the loss factor and a step in the absolute modulus. The effect of moisture-induced aging in glass beads of small size and the effect of sintering of ice grains in snow are investigated. The response of the pendulum is determined by the long-range statistical properties of force chains opposing the rotation of the pendulum, and by the tribological processes that take place at the grain contacts.

I. INTRODUCTION

This report is devoted to an experimental method devised to investigate the quasistatic mechanical properties of granular media. In the method the oscillating member of a low-frequency forced torsion pendulum is immersed into a granular medium, and the response to an applied harmonic torque is measured. We discuss the various aspects of operation of the pendulum and the data obtained in some prototype granular systems: glass beads, natural sand, and low-density granular snow. On one hand, this will provide the background for the proper exploitation of the method and, on the other hand, it will show the complex role of inhomogeneous force propagation in a collection of particles in contact from a different perspective.

II. A HIERARCHY OF PROBLEMS

This section gives a schematic, nonexhaustive view of the problems encountered in granular media in static and quasistatic conditions [1]. The complexity of the problem can be appreciated by observing the medium at different length scales. Assume that the grains have millimetric size, and zoom out from small to large length scales. At a nanometric to micrometric level one sees the asperities at the surfaces of two grains in contact. This is the ''microscopic'' length scale of the system, where a large variety of tribological processes arise. These processes give rise to microscopic forces which can be divided, according to Bowden and Tabor [2], into two types: (i) *adhesion* forces resulting from the formation of adhesive junctions between the surface asperities, such as van der Waals forces, solid bonds, capillary bridges; (ii) *deformation* forces that result from elastic and various inelastic processes in a relatively large subsurface volume, such as plastic and viscoplastic deformation, fatigue, surface fracture, and other forms of localized dissipative processes.

By zooming out to a millimetric length scale, the two interacting grains can be seen in full. The microscopic tribological forces emerge at this scale in the ''contact forces.'' In particular, some of the microscopic forces emerge in a contact force that is proportional to the normal load, i.e., a *fric-tion* force satisfying the usual Coulomb-Amontons law. The friction force can englobe deformation *and* adhesion microscopic forces, e.g., the adhesion forces that originate from water capillary bridges at nanometric asperities [3]. Other forms of microscopic forces, e.g., solid bonds between ice grains in snow [4], can emerge as load-independent *cohesion* contact forces, or depend on the load in a nonlinear way.

By continuing to zoom out, one reaches a ''mesoscopic'' length scale where one can see ten to one-hundred grains in contact. At this scale the problem of the transmission of the contact forces through a granular system appears. Because of the inhomogeneity of packing, size, and shape of the grains, the total force acting on a given grain is transmitted unevenly to the adjacent grains. In experimental conditions where all the contact forces are below the threshold for sliding, one observes that an increasing applied force causes strain to build up along ''force chains,'' i.e., a network of stress-transmitting paths involving only a fraction of the total grains [5]. Because the external force is concentrated over the small contact areas, the overall elasticity of the medium is strongly nonlinear [6]. When the contact force between a pair of grains becomes large enough for the two grains to start slipping one against the other, one moves to a complex quasistatic regime. Each single random slip event between two grains has repercussions at a *large distance* via the force-chain network, and the response of the granular medium involves the statistical redistribution of contact forces between a large number of grains. Moreover, if one imagines introducing a large object into the granular system and moving it slowly relative to the medium [7], at this length scale one observes a *fluctuating* force distribution resisting the motion: strain is built up and released between force chains trying to resist the motion of the object, giving a stick-slip character to the phenomenon [8].

Finally, by zooming out to the scale of the whole sample, what one sees is a solid body responding elastically to small applied forces, possibly fracturing or creeping under the effect of large external forces. At this ''macroscopic'' scale one naturally adopts a mean-field description [9] where the complex distribution of contact forces and of grain positions is averaged in a continuum stress-strain field. In the con-
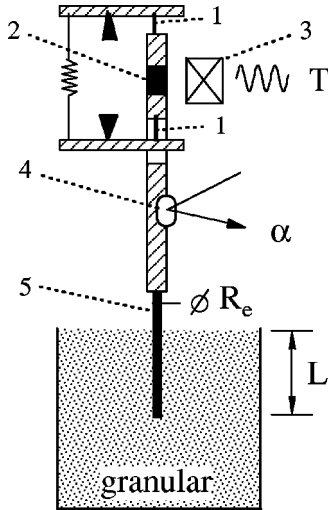
FIG. 1. Sketch of the forced torsion pendulum immersed into a granular medium. 1, suspension wires; 2, permanent magnet; 3, external coils; 4, mirror; 5, probe covered by a fixed layer of grains.

tinuum description the mechanical stability of a granular medium can be written in the form of the criterion $\tau < \mu_s \sigma + c$, where τ is the tangential stress across a plane within the granular medium, σ is the normal stress acting on the same plane, μ_s is the coefficient of static friction, and c is usually considered a macroscopic load-independent cohesion force per unit surface. The criterion imposes a limit, i.e., $\tau_f = \mu_s \sigma + c$, on the magnitude of the shear stress that can occur within the granular medium, beyond which contact forces are overcome and gross failure arises. Notice that the continuum description can in principle be used down to a small length scale of a few grain diameters. However, most of the mesoscopic physics is then lost, although the microscopic physics is retained in the coefficients μ_s and c.

III. EXPERIMENT

The torsion pendulum (Fig. 1) consists of a long cylinder able to freely rotate around its axis, but prevented from flexing sideways by two thin suspension wires fixed to the cylinder and under tension. Similar apparatuses are used in metallurgy and other physical systems [10]. The pendulum is forced into torsional oscillation by a time-dependent torque $T(t) = T_0 \exp(i\omega t)$ applied by using a small permanent magnet fixed to the pendulum and a pair of external coils where an ac current circulates. The angular displacement of the pendulum, $\alpha(t)$, is measured optically. The complex frequency response of the pendulum is obtained from $G(\omega) = T(\omega)/\alpha(\omega)$ using a lock-in device. In a typical measurement we record the argument $\arg(G_1)$ and the absolute modulus (*modulus* in short) $|G_1|$ of the first harmonic of the response, as a function of the amplitude of the applied torque T_0. We also record the argument and modulus of the third and fifth harmonics, denoted $\arg(G_3)$, $|G_3|$ and $\arg(G_5)$, $|G_5|$, respectively, at the same time. The damping properties of an oscillating system are well represented by the *loss factor* η, which is the dimensionless ratio of dissipated to stored energy per cycle. For linear systems $G \equiv G_1$, and the loss factor is given by $\eta \equiv \tan[\arg(G_1)]$. For strongly nonlinear systems as is the case here, as an approximation of the

loss factor we use the quantity $\eta \simeq \tan[\arg(G_1)]$ or $\eta \simeq \tan[\arg(G)]$ with $G = G_1 + G_3 + G_5$. The forcing frequency (1 Hz) is chosen well below the natural frequency of the pendulum (which is about 30 Hz). The loss factor of the suspension wires is of the order of 10^{-4}; thus the pendulum not immersed can be assumed elastic and the response reduces to $T(\omega) = G_p \alpha(\omega)$, where $G_p = 18 \times 10^{-3}$ N m/rad is a torsion constant.

In the experiments, the cylindrical probe is immersed at a given depth into a large bucket containing the granular material. The data presented here were obtained in glass beads of diameter $d_g = 1.1 \mp 0.05$ mm and $d_g = 70 \mp 10$ μm, with polished smooth surfaces, and in uncontaminated sand composed of multifaceted quartz grains with very homogenous size of about 160 ∓ 32 μm. The flat faces of the sand grains appear polished and very clean in the microscope. Other experiments were conducted in granular systems composed of glass beads of different sizes, and sand of various origins. (The specification concerning experiments conducted in granular snow will be presented in detail in Sec. VII.) Some specific experimental procedures have been adopted: First, we covered the probe by a layer of grains glued on by an epoxy and we took care as far as possible not to contaminate the external surface of the glued grains with the epoxy itself. Some experiments were also conducted with clean probe surfaces, as specified. Second, in order to discard effects due to the construction history of the system, the probe was pushed at some depth into the granular medium *fluidized* by strong external vibrations. Moreover, measurements were taken after a fixed time from the fluidization, which provided a way to handle moisture-induced aging effects. Such aging effects were observed at ambient humidity in granular systems composed of grains with sizes less than about 200 μm, but were almost absent for grains of larger size. Measurements were performed either at uncontrolled ambient humidity or under nitrogen atmosphere, as specified. Finally, the whole system was placed on an antivibrational table to prevent undesired vibration-induced effects.

IV. RESULTS

A. Glass beads

In measurements of the loss factor, approximately given by $\eta \simeq \tan[\arg(G_1)]$, and modulus $|G_1|$ as a function of the amplitude of the applied torque T_0, we systematically observed a mechanical behavior with a pronounced loss peak and a step in the modulus. Figure 2 shows such data obtained in glass beads with $d_g = 1.1 \mp 0.05$ mm using a cylindrical probe covered by a layer of glued beads, giving an effective radius of $R_e = 1.5$ mm, and extending below the surface for different lengths L. The loss factor displays a pronounced peak at a torque denoted T_0^* in Fig. 2(a). The modulus $|G_1|$ shows a step between two levels denoted G_p and G_{low}, respectively, in Fig. 2(b). These measurements were conducted in ambient humidity of 40%, but no difference was observed in the dry system. There was also no difference on decreasing or increasing amplitude.

Visual observations at the sample surface revealed that, at high torque amplitude, multiple grain slip events occurred randomly in a large area around the probe, and a localized
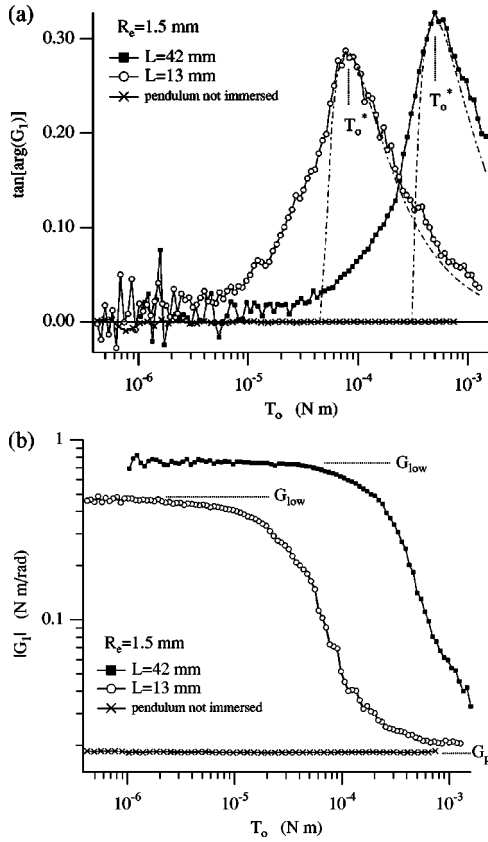
FIG. 2. The loss factor given approximately by $\eta \simeq \tan[\arg(G_1)]$ (a) and the modulus $|G_1|$ (b) versus the amplitude of the applied torque T_0, of the pendulum immersed into a granular system of glass beads 1.1 mm diameter at ambient humidity 40%. The probe is covered by a layer of glued spheres, giving an effective radius $R_e = 1.5$ mm, and is immersed at two different depths L. The point-dashed lines on the loss data are fitting lines obtained from a rheological model (see text). The position of the loss peak is denoted T_0^*. The modulus observed at low applied torque is denoted G_{low}. The response of the pendulum not immersed is also shown.

failure surface was not observed. Although the observations were with the naked eye, slip events could be detected, using appropriate illumination, at very large distance from the rotating probe, with distances of the order of some centimeters at least.

Since the mechanical behavior of Fig. 2 is very general, we also show here the dependence of the loss peak on the geometrical parameters of the experiment. Figure 3 shows the position of the peak T_0^* as a function of L for different R_e, obtained from measurements in dry glass beads with $d_g = 1.1 |\mp| 0.05$ mm, under nitrogen atmosphere. These data have been fitted by power laws of the form $T_0^* = aL^\beta$ with a and β free parameters: we obtain $\beta \approx 2.1$, 1.9, 2.0, 1.9, and 1.9 for $R_e = 3.5$, 3, 2.5, 2, and 1.5 mm, respectively. The point-dashed lines in Fig. 3 are the best quadratic fit to the data of the form $T_0^* = aL^2$. The inset of Fig. 3 shows the coefficients a obtained from the quadratic fit, versus R_e. The dashed line in the inset is a power-law fit of the form $a = bR_e^\alpha$: we obtain $\alpha = 2.1$. A quadratic fit gives $b = 1.5 \times 10^5$ N/m^3. Therefore, the data can be summarized by the empirical relation
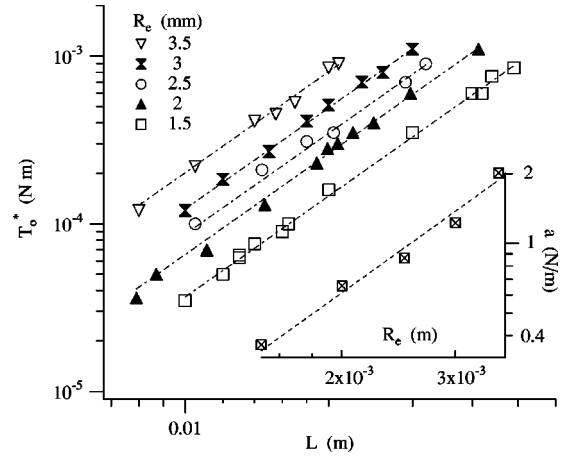

FIG. 3. The position of the loss peak T_0^* versus L, for various R_e, from data obtained in dry glass beads of 1.1 mm diameter, under nitrogen atmosphere. The point-dashed lines are quadratic fits of the form $T_0^* = aL^2$. Inset: The coefficient a of the quadratic fits in the main panel, versus R_e. The dashed line in the inset is a power-law fit of the form $a = bR_e^\alpha$ with $\alpha = 2.1$, and $b = 1.5 \times 10^5$ N/m^3 in a quadratic fit. These data support the empirical relation $T_0^* \propto L^2 R_e^2$.

$$T_o^* \propto L^2 R_e^2 \tag{1}$$

between the position of the loss peak and the dimensions of the probe.

For completeness we anticipate at this stage that the validity of this empirical relation is restricted to systems where macroscopic load-independent cohesion forces are absent or negligible, which is the case for the glass beads used here. In the snow system, solid bond adhesion forces between ice grains dominate and a different empirical relation is observed (Sec. VII). In the presence of moisture-induced aging effects in the glass beads and in the sand, the empirical relation remains valid provided these effects are properly taken into account, e.g., if the position of the peak is measured at the same aging time (Sec. VI).

B. Sand

A special experiment in sand is reported in Fig. 4 and Fig. 5 as an example of a different mechanical behavior from the one presented in the previous subsection. The difference arises because in this case experiments were conducted using clean copper cylinders (i.e., without the layer of glued grains). The data of Fig. 4 were obtained using a clean copper cylinder of radius $R = 1.5$ mm and extending below the surface for a length $L = 35$ mm. The experiment was conducted in ambient humidity of 35%. Measurements were obtained by increasing (up) and decreasing (down) applied torque, with no apparent difference. In addition to the argument and the modulus of the first harmonic, Fig. 4(c) also shows the inverse of the norm of the third and fifth harmonics, denoted $1/|G_3|$ and $1/|G_5|$, respectively, measured in parallel to the first harmonic. One can see the sharp onset of nonlinearity in the system in the region of the loss peak. The inset of Fig. 4(a) shows the loss peak with higher torque resolution; the peak culminates at about $\eta^* \approx 1.2$, corresponding to an argument $\arg(G_1)$ of more than 50°. The data
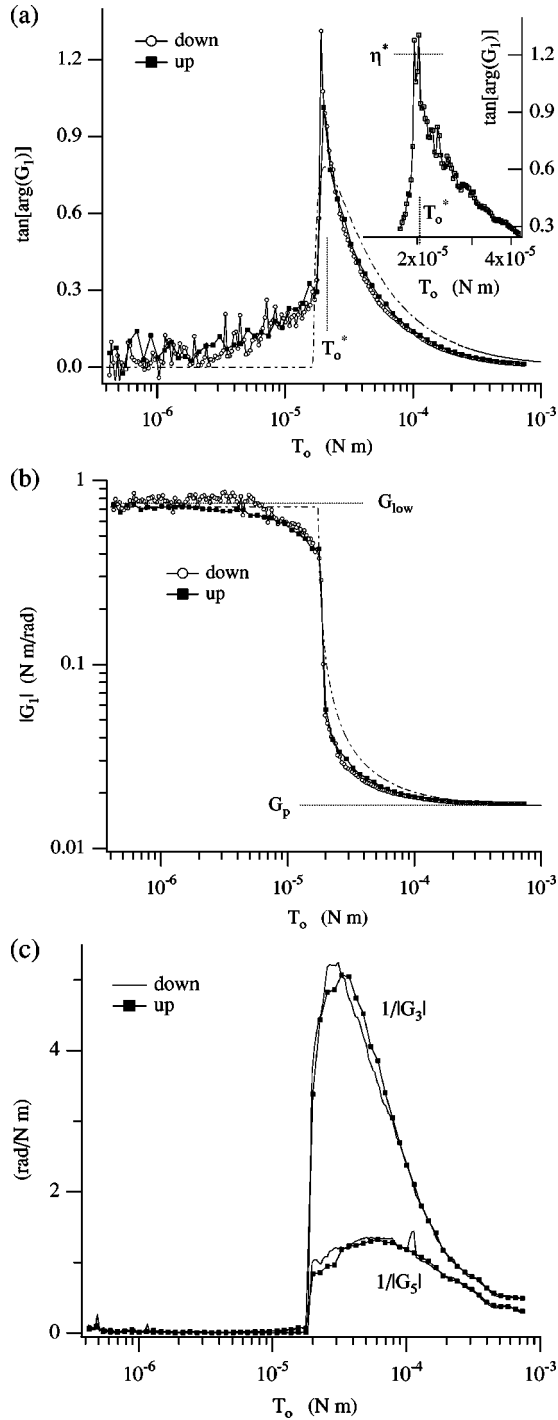
FIG. 4. $\tan[\arg(G_1)]$ (a), $|G_1|$ (b), and the inverse norm of third and fifth harmonics (c) of the torsion pendulum immersed into natural sand, for increasing (up) and decreasing (down) torque amplitude T_0. In this case the (clean) probe is a polished copper cylinder. The point-dashed lines are fitting lines according to the rheological model. Inset: The region of the loss peak measured with a higher torque resolution, showing a loss factor close to 1.2.

FIG. 5. The correction to the loss factor due to high harmonics of the response: (a) $\tan[\arg(G_1)]$ and $\tan[\arg(G_1+G_3+G_5)]$; (b) the corresponding modulus $|G_1|$ and $|G_1+G_3+G_5|$. The torsion pendulum (clean probe surface) is immersed into natural sand, and measurements are taken for decreasing torque amplitude T_0. The point-dashed lines are fitting lines according to the rheological model. The correction due to high harmonics influences the magnitude of the loss peak, but does not affect the position of the loss peak and the modulus.

very large argument, as is the case here, the correction to the magnitude of the loss peak is relevant.

Inspection of Figs. 4 and 5 shows a sharp increase just below the maximum. This behavior appears to be related to the specific failure mode for clean surfaces since visual observations revealed that a *localized* fracture occurred in the sand from just below the maximum to large amplitude. The failure apparently arose at the grain-probe interface. In Fig. 4 the progressive increase of the loss factor at low torque, below the peak, is related to delocalized grain slip events as in the glass beads.

V. MODELING

A. Rheological model

The observed mechanical behavior is captured by a simple rheological model [11] shown in Fig. 6(a). It is the simplest approximation of the pendulum immersed into a granular medium. In the model, the spring G_p represents the

of Fig. 5 were obtained using a clean copper cylinder of radius $R=2$ mm and $L=60$ mm. The humidity was about 45%. Figure 5 shows in particular the correction to the loss factor when high harmonics of the response are taken into account. The position of the peak and the absolute modulus are not affected by high-harmonic correction. However, for
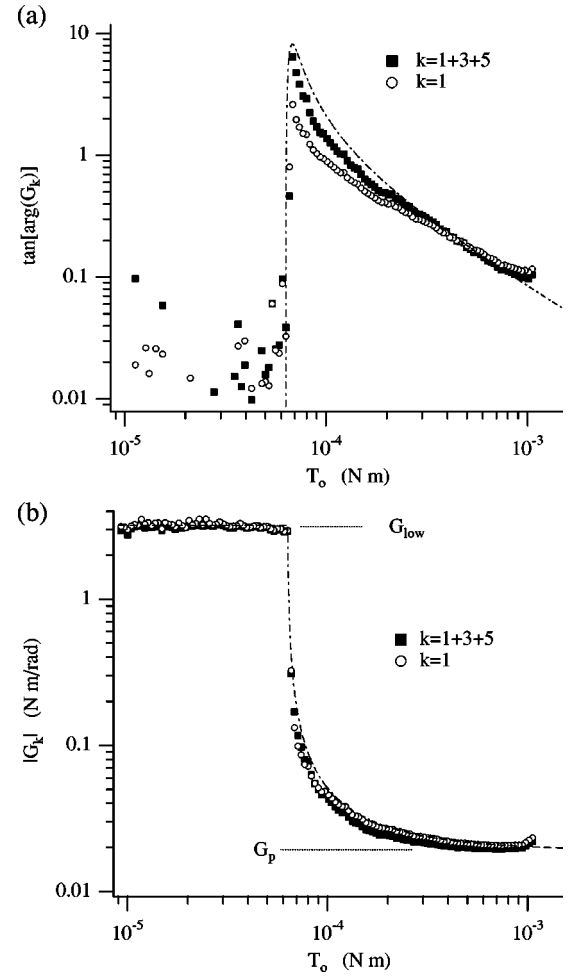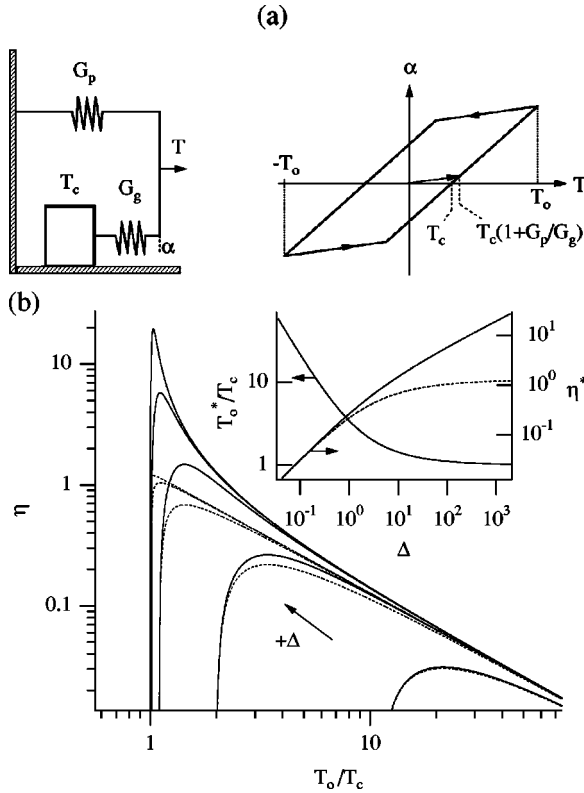
(a)

(b)

FIG. 6. (a) Rheological model and the hysteresis loop. The model is a simple approximation of the pendulum immersed into the granular medium. The lower branch represents the granular medium, characterized by a slide unit of critical torque T_c and a spring of torsion constant G_g. The upper branch represents the suspension wires of the pendulum, of torsion constant G_p. (b) The loss factor $\eta = Q/2\pi W$ calculated from the rheological model, plotted as a function of the normalized amplitude of the applied torque, T_0/T_c, for different Δ. Q is the damping energy per cycle (i.e., the area of the hysteresis loop) and W the strain energy per cycle. Different definitions of W are possible. The solid lines are calculated assuming W to be the elastic energy stored in the springs during loading (i.e., the area under the increasing branch of the hysteresis loop, starting from $\alpha=0$, $T=0$). The dashed lines are calculated assuming W to be the area under the secant modulus. The various curves correspond to an increasing Δ of 0.1, 1, 10, 100, and 1000, respectively. Inset: The position T_0^*/T_c and the magnitude η^* of the loss peak as a function of Δ, for the two definitions of the strain energy. At large Δ, the position of the peak is approximately given by $T_0^* \approx T_c$.

suspension wires of the pendulum, while the other branch represents the granular medium, characterized by a *slide unit* with a critical torque T_c and a *spring* of torsion constant G_g. The "mesoscopic" significance of the critical torque T_c will be discussed at the end of this section. The response of the slide unit alone is nonlinear and given by $\alpha=0$ for $T<T_c$ and by the constant $T=T_c$ otherwise. The hysteresis loop of the model is also shown in Fig. 6(a). Notice that the critical torque on the slide unit is reached when the applied torque is equal to $T_c(1+G_p/G_g)$.

The loss factor is the relative damping energy per cycle of the applied torque, given by $\eta=Q/2\pi W$, where Q is the damping energy per cycle and W the strain energy per cycle. Q is the surface of the hysteresis loop in Fig. 6(a). The definition of the strain energy is not unique and different criteria

can be used; here we define W as the elastic energy stored in the two springs during loading. We adopt the notation $\Delta = G_g/G_p$, and we introduce the normalized torque amplitude $f=T_0/T_c$, as well as the auxiliary variables $y = f\Delta/(1+\Delta)$ and $z=1/y$. Simple algebra shows that the loss factor can be written

$$\eta = \frac{4\Delta}{\pi} \frac{y-1}{2y-1+(1+\Delta)(y-1)^2} \quad (2)$$

for $y>1$, and $\eta=0$ for $y\leq1$. Equation (2) is a peak with maximum occurring at the normalized torque given by $f^* = (1+\Delta+\sqrt{1+\Delta})/\Delta$, which has the limits $f^*=1$ for $\Delta \gg 1$ and $f^*=2/\Delta$ for $\Delta\ll1$. In practice one can use the approximation $f^*\approx(2+\Delta)/\Delta$. Accordingly, the position T_0^* of the peak can be very large compared to T_c if Δ is small. However, the observed values of Δ in this work are $10<\Delta$, and we can assume $T_0^*\approx T_c$. The loss peak (2) is shown in Fig. 6(b) as a function of T_0/T_c and for different Δ. The magnitude of the peak is

$$\eta^* = \frac{2\Delta}{\pi}(\sqrt{1+\Delta}+1)^{-1} \quad (3)$$

where η^* tends toward $2\sqrt{\Delta}/\pi$ for $\Delta\gg1$ and toward Δ/π for $\Delta\ll1$. The inset of Fig. 6(b) shows the normalized position of the loss peak $f^*=T_0^*/T_c$ and η^* as a function of Δ. [Figure 6(b) also shows the result obtained with a different definition of the strain energy [12].] The absolute modulus, $|G|$ can be obtained from the slope of the secant modulus, which gives

$$|G| = \frac{(1+\Delta)G_p}{1+\Delta(1-z)} \quad (4)$$

for $z\leq1$ and $|G|=(1+\Delta)G_p$ for $z>1$. Equation (4) represents a step between the two levels G_p+G_g and G_p.

The rheological model provides a first, macroscopic understanding of the observed mechanical behavior. The low-torque modulus G_{low} can be identified with G_p+G_g in the model. Since $G_g\gg G_p$ the low-torque modulus is a direct measure of the elastic parameter G_g. The modulus at large torque coincides with the torsion constant G_p as measured for the pendulum not immersed into the granular medium. Since $\Delta\gg1$ (e.g., of the order of 40 for $L=42$ mm in Fig. 2) the position of the peak T_0^* can be identified with T_c in the model. An empirical approach to the analysis of the data consists in extracting Δ, and thus G_g, from the modulus step using $G_{low}\approx G_g$ and T_c from the position of the loss peak using $T_0^*\approx T_c$.

Fitting the data to the rheological model is in general only relatively satisfying, although the observed mechanical behavior is close to the rheological one. In particular, the sharp onset predicted by the rheological model is observed only when the probe surface is clean, as is the case for experiments in sand. Difficulties arise also concerning the magnitude of the loss peak at large Δ due to the correction for high harmonics. Very good accord between the rheological model and the data is, however, obtained in Fig. 5, where the loss factor is approximated by $\eta\simeq\tan[\arg(G)]$ with $G=G_1 +G_3+G_5$ and the modulus by $|G_1+G_3+G_5|$. In particular,

the modulus in Fig. 5(b) is fitted with Eq. (4) with Δ, T_c, and G_p as free parameters. We obtain $\Delta = 167$, $G_p = 0.018$ N m/rad, and $T_c = 6.3 \times 10^{-5}$ N m. The point-dashed line in Fig. 5(a) is obtained with Eq. (2) with the parameters Δ and T_c obtained from the modulus fit. The point-dashed lines for the loss data in many other figures are fitting lines obtained with Δ and T_c as free parameters. In general, the Δ obtained from the loss data is much less than the Δ obtained from the modulus. Further development is necessarily at the rheological level, possibly by exploiting theoretical advances obtained in other classes of materials [13], like suspensions in liquids or plasticity of metals.

B. Mesoscopic picture

In the rheological model the critical torque is the limit beyond which energy dissipation sets in. As a macroscopic approximation of the real process, the pendulum probe has be seen as sliding in the granular medium, in a similar way as a macroscopic body slides over a large surface. We try now to give a mesoscopic picture of this process.

1. Continuum approach

In the continuum approach [9], $\tau_f = \mu_s \sigma + c$ is the failure limit of the shear stress that can been reached across a plane within the granular medium, beyond which contact forces are overcome. The critical torque in the rheological model can be seen as the *macroscopic failure limit*, i.e., $T_c = T_f$. We postulate that the failure occurs homogeneously along a cylindrical vertical surface, in close proximity to the first layer of grains fixed on the probe surface [14], at the radius R_e (although visual observations do not reveal in general such a localized failure surface.) For glass beads and natural sand a reasonable assumption is that there are no macroscopic load-independent cohesion forces acting between the particles (see also the discussion of moisture-induced aging effects in Sec. VI), so that the continuum criterion reduces to

$$\tau_f = \mu_s \sigma. \qquad (5)$$

The macroscopic failure limit T_f can be obtained by considering that on a vertical plane at a depth x from the surface of the granular medium $\tau_f(x) = \mu_s \sigma(x)$, where μ_s is the coefficient of static friction, and $\sigma(x) = K \rho g x$ is the pressure acting in the horizontal direction, with ρ the granular density, g the acceleration of gravity, and K a constant that characterizes the pressure anisotropy [15,9]. The failure torque on a slice of area $2 \pi R_e dx$ of the cylindrical failure surface is $2 \pi R_e^2 \tau_f(x) dx$ at the depth x. Integrating along the probe of length L, we obtain

$$T_f = \eta_f \rho g L^2 R_e^2 \qquad (6)$$

where $\eta_f = \mu_s K \pi$ [16].

2. Discrete approach

In a discrete picture we need to take into account explicitly the complexity of force transmission in granular media. The main question is, *what is the force distribution opposing the rotation of the pendulum at a given moment during the cycle?* Due to the geometry, and considering that the first
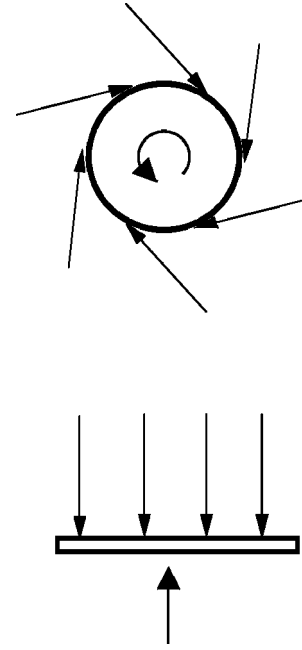

FIG. 7. Schematic distribution of force chains opposing the rotation of the pendulum (top) and opposing the straight motion of an immersed object (bottom). The top distribution is postulated in order to develop a picture of the mesoscopic origin of the pendulum response. In the presence of a layer of grains fixed to the probe surface (this arises if the layer is glued artificially to the probe surface, or if the friction force at the grain-probe interface is large enough), the force opposing the rotation of the pendulum results from compressive stress accumulated in force chains oriented along trajectories quasitangent to the probe. Shear stress at grain contacts oriented in the radial direction is assumed not to play a significant role.

layer of grains is firmly fixed to the surface probe, the spatial force distribution is likely to be organized along directions almost *tangent* to the cylindrical probe, where maximum strain can be built up between chains of grains, as sketched in Fig. 7 (top). The implicit assumption of the picture is that shear stress at grain contacts oriented in radial directions does not play any significant role compared to the compressive stress supported by chains of grains aligned along quasi tangent trajectories originating from the fixed grains. Because force chains essentially support compressive stress, the torque resisting the rotation has a similar origin to the drag force opposing the straight motion of an immersed object (Fig. 7, bottom), i.e., the random *buckling* of force-chains in front of the object, where compressive stress is continuously built up and released.

For an immersed solid object moving straight forward the drag force F_d has been shown by Albert *et al.* [7] to be velocity independent. Therefore we postulate a rate-independent drag torque T_d resisting the rotation of the pendulum, and we look for $T_c = T_d$. This approach gives us the opportunity to directly exploit the model and the result obtained in Ref. [7].

We divide the system into $n = L/d_g$ discrete horizontal layers of thickness d_g. A given layer i is stable, or ''elastic,'' until the local force between a pair of grains somewhere in the layer is larger than a critical *friction* force F_c, above which the two grains slip relative to each other. The inho-

mogeneous force distribution is incorporated into the problem by calculating, first, the probability that in a given discrete layer the local force exceeds F_c, and, second, the probability that the local force exceeds F_c in all the discrete layers *simultaneously*, which is the requirement for the pendulum to be able to rotate relative to the granular medium. In our case the source of the force on a layer is the grains fixed on the circumference of the probe such that the rotating cylinder of radius R_e is equivalent to an object of transverse size $2\pi R_e$ moving straight forward, which leads to the drag torque

$$T_d = \eta_d \rho g L^2 R_e^2, \tag{7}$$

where $\eta_d = \mu_s K 2\pi\sqrt{32\pi^2/27e^2}$ [16]. The drag torque is related to the drag force of Ref. [7] by $T_d = F_d R_e$. The factor $\mu_s K$ results from the local pressure in the horizontal direction controlling the critical friction force F_c.

3. Discrete versus continuum approach

The two approaches predict a quadratic L and R_e dependence. This result *is in agreement with the empirical relation* (1) obtained in Sec. IV. Although the two approaches give a similar result, the mesoscopic picture is very different. In the continuum approach the failure occurs over a definite surface, where the failure shear stress is overcome. In the picture, the two parts of the fractured granular medium are only elastically deformed, and no grain slip events arise except at the failure surface. In the discrete approach there is no localized failure, in the sense of the continuum description. Slip events can arise at large distances from the rotating probe. Moreover, the implicit assumption of the discrete picture is that the rigidity of the medium is provided essentially by force chains supporting compressive stress, and the medium is ''fragile'' [17]. Notice that Eqs. (6) and (7) differ by a numerical factor $\eta_d/\eta_f \approx 2.5$, possibly related to the different mesoscopic picture.

The continuum and discrete models also predict a critical torque proportional to the coefficient of static friction. This will permit a further check on the validity of the mesoscopic picture by artificially changing the friction properties of the system in the next section. Equations (6) and (7) also show that the position of the loss peak can in principle be used to measure the coefficient of static friction. From the fitting parameter $b = 1.5 \times 10^5$ N/m^3 in Fig. 3, the measured granular density $\rho = 1.6 \times 10^3$ kg m^{-3}, and using $b = \eta_i g \rho$ ($i = f, d$), we obtain $\eta_i \approx 9.6$. This gives $\mu_s K \approx 1.2$ from Eq. (7) and $\mu_s K \approx 3$ from Eq. (6). Using $K = 0.33$ one obtains 3.6 and 9.1, respectively, as an estimate of the friction coefficient.

VI. AGING EFFECTS

For glass beads with sizes less than about 200 μm, moisture-induced aging effects were observed at ambient humidity. According to Bocquet *et al.* [3], water capillary bridges nucleate at nanometric surface asperities between glass beads, providing a logarithmic time-dependent coefficient of static friction

$$\mu_s(t_a) = \mu_{s0} + A\ln(t_a/t_0) \tag{8}$$

where t_a is the aging time, t_0 is a microscopic time, and A is a constant related to the relative partial pressure of the fluid, the dimension of the nanometric asperities, the liquid-vapor surface tension, and some other geometric factors characterizing the surface roughness. The coefficient μ_{s0} is the coefficient of static friction that characterizes the dry granular medium. Notice that in the model of Bocquet *et al.* [3] the capillary force that emerges at mesoscopic scale is proportional to the normal load and therefore this contact force satisfies the Coulomb-Amontons law of static friction. Accordingly, the moisture-induced aging effect has to be included in the coefficient of static friction. This justifies the former assumption, Eq. (5), that the continuum criterion reduces to $\tau_f = \mu_s \sigma$ for the glass beads in question.

To control the aging effect experimentally, we exploited the fact that capillary bridges are destroyed during the fluidization of the granular medium. After fluidization, the capillary bridges will grow again with the logarithmic time dependence of the resulting friction force. We conducted experiments in glass beads with $d_g = 70 \mp 10$ μm, at ambient humidity of 40%. Figure 8 shows the loss peak and the modulus measured at different aging times t_a, where t_a is the time elapsed from the fluidization procedure. For this particular experiment, the fluidization-induced disaggregation procedure was repeated *before each point* on a curve, so that a single curve was obtained strictly after the same aging time. Notice that, during the imposed aging time, the pendulum continuously oscillates at the given torque amplitude (see Sec. VIII for a discussion of this point). The inset of Fig. 8(a) shows T_0^* as a function of t_a, and the point-dashed line demonstrates that the data align on a straight line in the lin-log plot, supporting the theoretical result that the position of the loss peak is proportional to the coefficient of static friction. The inset of Fig. 8(b) shows that the ''elastic'' parameter G_{low} also has a logarithmic time dependence.

A. More aging effect data

Figures 9(a) and 9(b) show more data obtained in the system of glass beads of 70 ∓ 10 μm diameter, with $R_e = 1.75$ mm and for different L, at ambient humidity of 35%. In this case the vibration-induced disaggregation procedure was repeated before each curve (and not before each point), so that the aging time at which the loss peak is observed is different for each curve, as indicated.

Figure 9(c) shows the position of the peak T_0^* as a function of L, obtained from Fig. 9(a), as well as the position of the peak extrapolated as if it were observed at a unique aging time of 1000 s. The solid and point-dashed lines in Fig. 9(c) are the best power-law fit to the data of the form $T_0^* = aL^\beta$. We obtain $\beta \approx 1.7$ for the data obtained without taking into account the aging time, and $\beta \approx 2.0$ for the data corrected for the aging time. This example shows that aging effects have to be considered carefully in the analysis, otherwise an incorrect L or R_e dependence could be observed.

VII. SNOW

We present here some data obtained in snow, i.e., ice grains in contact, although we are aware that natural snow can be seen as a granular medium only in certain conditions
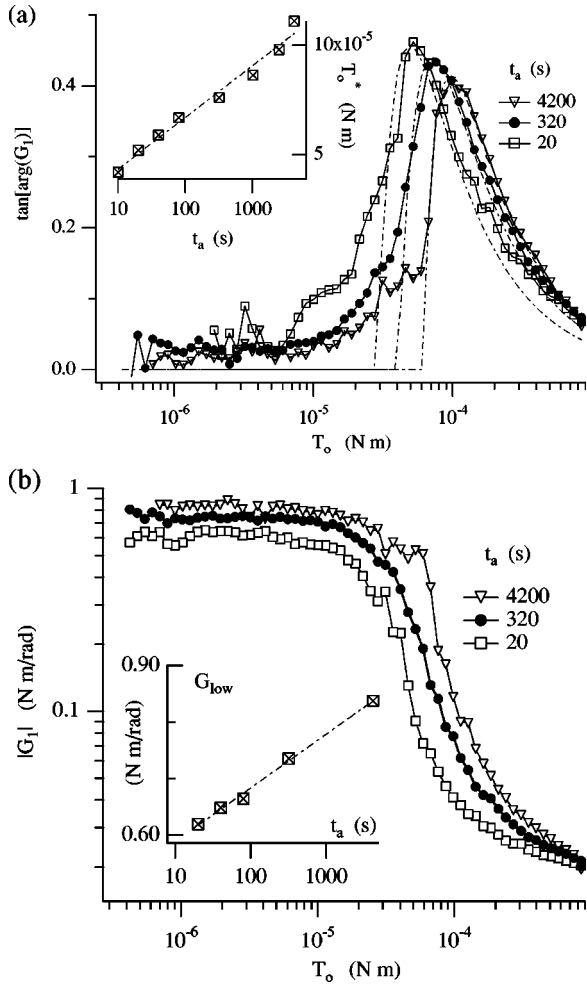
FIG. 8. $\tan[\arg(G_1)]$ (a) and $|G_1|$ (b) measured in glass spheres of 70 μm diameter at ambient humidity 40%, for different aging times t_a ($R_e = 1.75$ mm, $L = 19$ mm). t_a is the time elapsed from the fluidization of the granular medium, a procedure that disaggregates the grains. The vibration-induced disaggregation is performed before each point. The point-dashed lines in (a) are fitting lines obtained from the rheological model. Inset (a): The position of the loss peak T_0^* versus the aging time t_a. The data align on a straight line in the linear-logarithmic plot, showing a logarithmic time dependence of the form $T_0^* = c + p \ln t_a/t_0$, typical of the moisture-induced aging effect. Inset (b): Similar logarithmic time dependence of the low torque level G_{low}.

[4,18]. However, under the appropriate experimental conditions, this system provides an example of a granular medium controlled by *solid bonds*, as opposed to the usual granular systems where adhesion is commonly of capillary origin, thus illuminating the problem from another perspective. In fact, as soon as snowflakes are in contact, crystalline bonds between ice grains grow very rapidly in time. This "sintering" process introduces a time-dependent cohesion term $c(t_s)$ which is expected to rapidly dominate the friction term. This means that the continuum criterion reduces to

$$\tau_f = c(t_s), \qquad (9)$$

where t_s is the sintering time and $c(t_s)$ is the snow "shear strength," which can be assumed independent of the load in a first approximation.
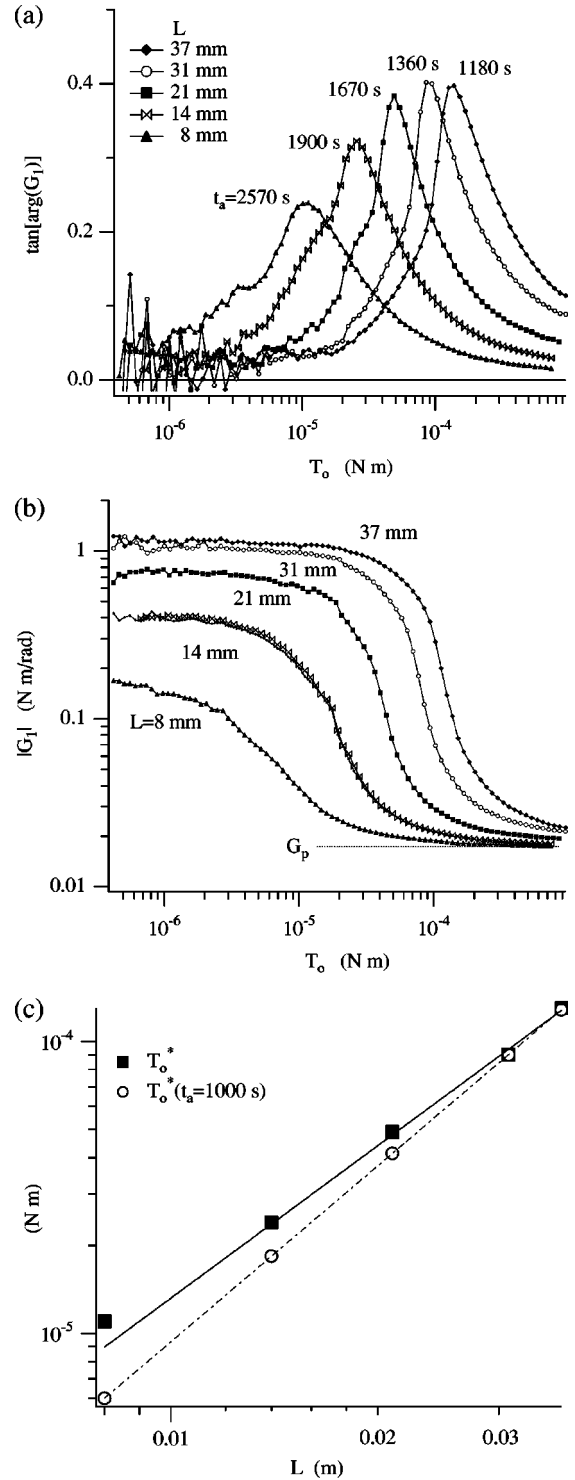
FIG. 9. $\tan[\arg(G_1)]$ (a) and $|G_1|$ (b) of the same granular system as in Fig. 8, for different L. In this case the vibration-induced disaggregation is performed before each curve, so that the loss peak is observed at different aging times, as indicated. (c) The position of the peak T_0^*, as a function of L, as well as the position of the peak extrapolated to a given equal aging time of $t_a = 1000$ s. The solid and point-dashed lines are power-law fits. For the position of the peak corrected to equal aging time we obtain a power of 2.

Because of the sintering process, granular snow differs from other granular systems in two respects: (1) The volume fraction of snow is very low. For example, we use low-density snow which approximately gives a volume fraction
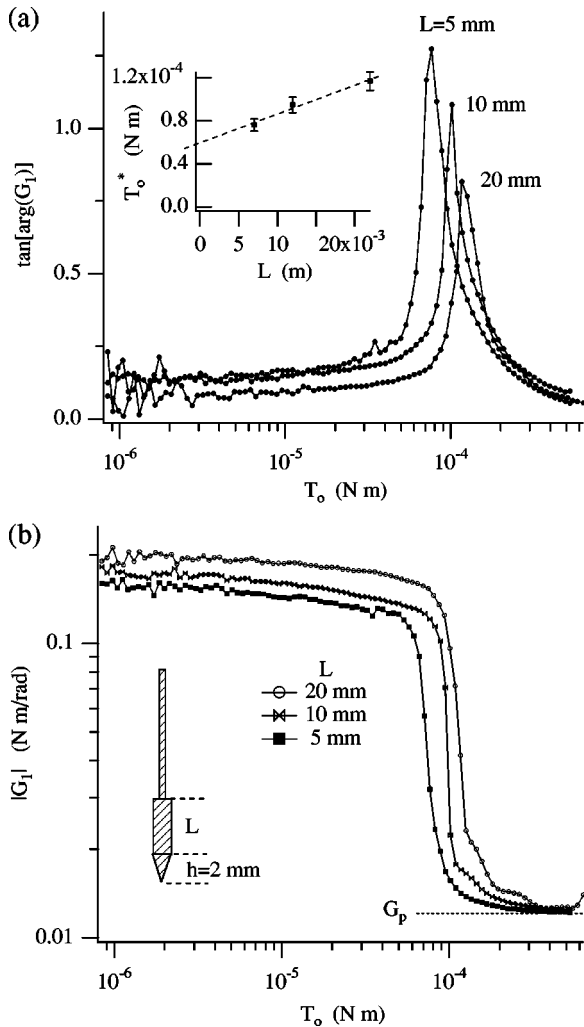
(a)

(b)

FIG. 10. The loss factor given approximately by $\eta \simeq \tan[\arg(G_1)]$ (a) and the modulus $|G_1|$ (b) of the pendulum immersed into low-density granular snow, using three different probes shown in (b). The experimental details are given in the text. Inset (a): the position T_0^* of the loss peak as a function of L.

$\nu = \rho_{snow}/\rho_{ice} \approx 0.28$. This has to be compared to the volume fraction of monodisperse three-dimensional packing of spheres, which is 0.74 for the crystal, 0.64 for the random close packing limit, and 0.57 for the random loose packing limit. The usual volume fractions for granular media are therefore around 0.6, so that a snow system is mostly composed of air. (2) The rearrangement of ice particles under gravity cannot occur. As shown by everyday experience, a cavity produced in the snow, e.g., by introducing a probe, will remain after the probe is extracted.

For these reasons, we have used specific probes for experiments in the snow system. The probes are clean copper cylinders of length L and terminating in a cone of height h, as shown in the inset of Fig. 10(b). In a typical experiment, the probe is pushed into the snow at a velocity such that the penetration is brittle [4]. That means that the bonds between the ice grains colliding with the probe are broken. These grains will be pushed aside by the conical point. As discussed, for example, by Fukue [4], one expects the formation of a zone of high-density snow in front of the conical section, and a similar layer along the cylindrical section. The

high-density snow layer is strongly bound to the cold, metallic probe surface, and the pendulum method measures properties *intrinsic* to the snow system, instead of grain-probe interface properties. Small deviations from the straight trajectory during the penetration in the inhomogeneous medium can reduce or locally break the contact between the high-density layer and the cylindrical section of the probe. As a consequence, one expects the main contribution to the pendulum response to come from the conical part of the probe.

A. Results

Figure 10 shows data measured in granular snow using three different probes. The probes are of length $L = 20$ mm, 10 mm, or 5 mm, with radius $R = 1.5$ mm and terminating in a cone of height $h = 2$ mm. Experiments were performed in a cold room, at $-13° \mp 0.1°$, such that the temperature of the samples and of the apparatus was the same and very homogenous. Data were obtained in snow samples composed of two-week-old grains. The snow was disaggregated and gently poured into a cylindrical aluminum container of about 20 cm diameter, 15 cm height. The density was $\rho = 270$ kg/m^3 and the average grain diameter was $d_g \approx 0.1$–0.2 mm. The pendulum was lowered and the probe was immersed into the sample in such a way that the conical part was at about $x = 30$ mm from the surface. (For the snow we do not use the fluidization procedure.) The speed of the immersion was of the order of 5 mm/s. The snow sample had sintered for about 17 h and each curve was obtained by immersing the probe in another location in the sample.

As for the other granular systems discussed above, we observe in Fig. 10 a large loss peak and a step in the modulus, in close similarity with the mechanical behavior of the rheological model. Notice, however, that the loss peak is narrower than in the glass beads and in sand.

The mechanical behavior of Fig. 10 can be understood in the framework of the continuum approach (Sec. V) taking into account that the continuum criterion for this system reduces to $\tau_f = c(t_s)$ and considering that the failure plane is composed of a cylindrical section plus a conical one. We obtain

$$T_f \approx c(t_s)2\pi R^2 L + c(t_s)2\pi R^2 h/3 \qquad (10)$$

with a characteristic linear dependence on L. This is different from the L^2 dependence obtained in the glass beads. Such a different L dependence could be used to distinguish experimentally whether friction or cohesion forces dominate in a given granular system.

The inset of Fig. 10(a) shows the position T_0^* of the three peaks versus L. The three points align on a straight line which intersects the vertical axis at $L = 0$ at about 6×10^{-5} N m. By extrapolating the fitting line to $L = 0$ and using Eq. (10), we obtain $c(t_s) \approx 6$ kPa where $t_s = 17$ h. The usual values of the snow shear strength in the literature [18,19] for similar snow density are in the range of 1 kPa to 10 kPa, in accordance with the value determined here. We can obtain an estimate for the shear strength also from the slope of the fitting line in the inset of Fig. 10(a), which gives a value of 0.2 kPa, i.e., one order of magnitude smaller than previously. This result confirms that the relevant contribution to the shear strength comes from the final conical section of the
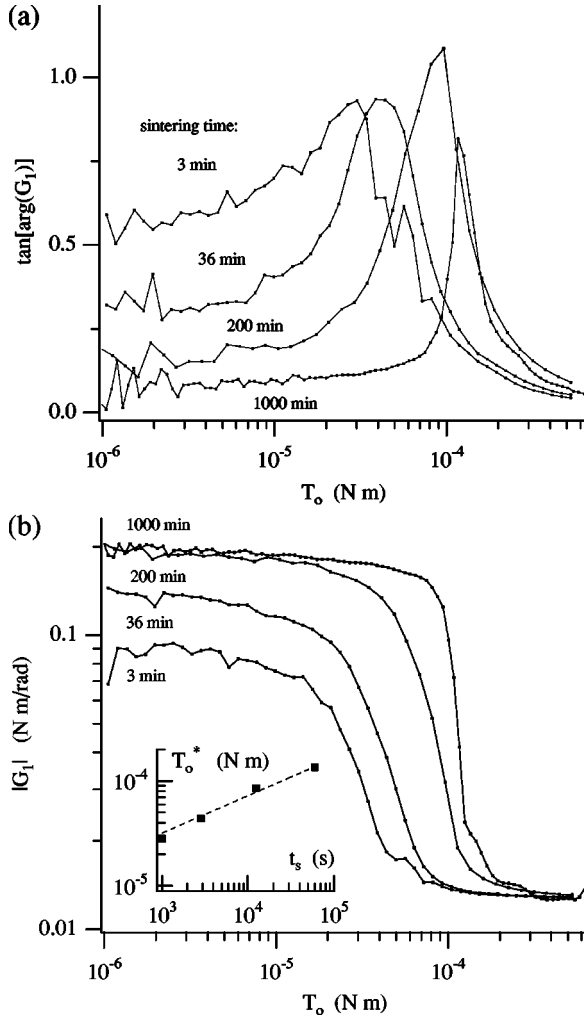
FIG. 11. Effect of snow sintering on $\tan[\arg(G_1)]$ (a) and $|G_1|$ (b), for different sintering time t_s of initially disaggregated, two-week-old grains. Inset: the position of the loss peak T_0^* as a function of the sintering time where the peak is observed. The dashed line is the best fit to the data of the form $T_0^* = At^\delta$. We obtain $\delta = 0.36$, i.e., a time dependence close to the theoretically predicted $t^{0.25}$ dependence for the growth of ice bonds by Colbeck [21] (see details in text).

probe and that the contact with surrounding snow grains is reduced along the cylindrical section compared to the conical part. The immersed pendulum method appears well adapted to performing field experiments in very low-density (fresh) snow, where other methods are impractical [20].

B. Sintering effect

The mechanical properties of the snow system are expected to be very sensitive to the overall sintering state. Figure 11 shows measurements performed at different sintering times. In the present experiment the snow (the same as that used for Fig. 10) was disaggregated and gently poured into the container. Immediately after the preparation (about 3 min) the probe ($L = 20$ mm) was immersed into the sample and a first measurement as a function of T_0 (by decreasing the torque) was obtained. A single measurement takes about 30 min. Successive measurements were then obtained after 36 min, 200 min, and 1000 min. As demonstrated by Fig. 11,

the response depends on the sintering state of the sample: the longer the sample was sintered, the larger the torque T_0^*.

The inset of Fig. 11(b) shows the position of the loss peak T_0^* as a function of the sintering time, taken at the time when the peak is observed. (For example, even if the first measurement starts only 3 min after the sample preparation, the peak is observed about 16 min later. The procedure is similar to that for the aging effect experiment of Fig. 9.) The dashed line in the inset of Fig. 11(b) is the best fit to the data of the form $T_0^* = At_0^\delta$. We obtain the exponent $\delta = 0.36$. A logarithmic fit is not satisfying, although, because of the small number of data points, the conclusions are only indicative. Accordingly, the time evolution of the snow shear strength can be approximated by a power law of the form $c(t_s) \propto t_s^{0.36}$. This time dependence is indeed close to the predicted $t_s^{0.25}$ dependence for the growth of ice bonds by Colbeck [21], giving credit to the approach discussed here.

We underline, however, that the validity of the picture is restricted to the conditions of our experiment, in particular, low temperatures, low-density snow, low frequency. In other conditions, the viscoplastic deformation of the ice bonds, as well as the thin layer of water formed by frictional heating, must be considered. In particular, due to stress-induced melting of the ice bonds, the loss factor measured by the pendulum close to 0° temperature can be much larger than for pure friction processes. In general, the question of the evolution of the magnitude of the loss peak has not been addressed, although it may contain valuable information on the system.

VIII. DISCUSSION AND OPEN QUESTIONS

Aging and sintering experiments have shown that the position of the loss peak is proportional to the coefficient of static friction in glass beads and sand, or proportional to the macroscopic shear strength in snow, i.e., $T_0^* \propto \mu_s$ or $T_0^* \propto c$, respectively. This is indeed very surprising for the following reason: During a long aging time, e.g., the data in Fig. 8, the pendulum continuously oscillates at the forced frequency of 1 Hz. At a torque amplitude just below and above the loss peak, one expects that the capillary bridges are continuously broken during the applied cycle. For many grain contacts the effective aging time can be no longer than the period of the oscillations. *How can the pendulum detect friction forces that correspond to aging times much longer than the oscillation period*? The same question arises for the sintering of snow. At large enough torque amplitude, the ice bonds are continuously broken and one expects the maximum sintering time to be limited to about the cycle period.

Although we do not have a definitive answer, we speculate that the long-term time dependence of the aging or sintering effects is observed in practice because the pendulum response *does not result from localized phenomena* in the granular medium. The inhomogeneous and fluctuating force distribution along force chains *delocalizes* quasistatic phenomena, in principle, to the entire medium. A slip event between two grains occurring somewhere within the granular medium has repercussions, via the force-chain network, at large distances. This large-scale reorganization of the grains that follows a slip event involves a large volume of the medium in the response. As a consequence, aging or sintering

effects, or in general any evolution in the tribological processes, can be detected.

Recently, mesoscopic theories have been built that take the inhomogeneous force distribution into account as a key factor, e.g., the q model [22] and the jamming theory [17]. We believe the present work to underline the necessity to extend and improve this newly developed understanding to quasistatic, dissipative regimes. Pendulum experiments in glass beads or low-density snow show that the method is well adapted to studying and developing notions like ''fragility'' and force-chain-induced ''jamming'' in quasistatic conditions.

This work is focused on the regime where the grains slip relative to each other, but the pendulum apparatus also provides information about the elastic properties of granular media. All the data presented show that at small applied torque the loss factor is small, and the modulus is independent of the applied torque. Under these conditions one can consider the granular medium macroscopically as an elastic body, and the pendulum response is a measure of an elastic modulus. Therefore, the dependence of the granular elasticity on the various tribological parameters could also be investigated.

IX. CONCLUSIONS

The pendulum response displays a characteristic mechanical behavior, with a peak in the loss factor and a step in the absolute modulus. The position of the peak can be used to measure the coefficient of static friction in macroscopically cohesionless granular systems, like glass beads, or to measure the shear strength due to ice bonds in granular snow. The analysis of the response of the oscillating probe provides, in general, information about tribological processes and characterizes the quasistatic state of the granular medium. When the particles, either glass beads or ice grains, are solidly bound to the probe surface, the pendulum probes the long-range statistical properties of force chains opposing the rotation. The general picture that has been developed shows the potential of the method for further developments in the understanding of granular mechanics at the mesoscopic level.

ACKNOWLEDGMENTS

[1] See, for example, H. M. Jaeger, S. R. Nagel, and R. P. Behringer, Rev. Mod. Phys. **68**, 1259 (1996).

[2] F. P. Bowden and D. Tabor, *The Friction and Lubrication of Solids*, 4th ed. (Clarendon Press, Oxford, 1986).

[3] L. Bocquet, E. Charlaix, S. Ciliberto, and J. Crassous, Nature (London) **396**, 735 (1998); J. Crassous, L. Bocquet, S. Ciliberto, and C. Laroche, Europhys. Lett. **47**, 562 (1999).

[4] M. Fukue, *Mechanical Performance of Snow Under Loading* (Tokai University Press, Tokyo, 1979).

[5] P. Dantu, Geotechnique **18**, 50 (1968); A. Drescher and G. De Josselin De Jong, J. Mech. Phys. Solids **20**, 337 (1972); T. Travers *et al.*, Europhys. Lett. **4**, 329 (1987).

[6] J. D. Goddard, Proc. R. Soc. London, Ser. A **430**, 105 (1990), and references therein.

[7] R. Albert, M. A. Pfeifer, A.-L. Barabási, and P. Schiffer, Phys. Rev. Lett. **82**, 205 (1999).

[8] B. Miller, C. O'Hern, and R. P. Behringer, Phys. Rev. Lett. **77**, 3110 (1996); S. Nasuno, A. Kudrolli, and J. P. Gollub, *ibid.* **79**, 949 (1997).

[9] R. M. Nedderman, *Statics and Kinematics of Granular Materials* (Cambridge University Press, Cambridge, 1992).

[10] A. S. Nowick and B. S. Berry, *Anelastic Relaxation in Crystalline Solids* (Academic Press, New York, 1972); G. D'Anna and W. Benoit, Rev. Sci. Instrum. **61**, 3821 (1990).

[11] B. J. Lazan, *Damping of Materials and Members in Structural Mechanics* (Pergamon, Oxford, 1968).

[12] The question of the definition of the strain energy in nonlinear rheological models has been widely debated, since a different definition of W results in a very different limit of the loss factor peak magnitude for large Δ. For example, defining the strain energy W as the area under the secant modulus, the magnitude is given by $\eta^* = 4(\sqrt{1+\Delta}-1)^2/\pi\Delta$, which tends toward the constant $4/\pi$ for $\Delta \gg 1$. The position of the loss peak is, however, the same as that obtained in Sec. V A.

[13] See, for example, D. Doraiswamy, A. N. Mujumdar, I. Tsao, A. N. Neris, S. C. Danforth, and A. B. Metzner, J. Rheol. **35**, 647 (1991).

[14] In the case where the probe surface is clean, we must distinguish the two cases where the grain-probe friction is larger or smaller than the grain-grain friction, respectively. Having a glued grain layer on the probe corresponds to an almost infinite grain-probe friction.

[15] The use of a hydrostatic pressure means that we assume the dimensions of the container to be large compared to L and R, which is always the case in our experiments. We also make the simplification not to distinguish the active and passive granular states. This is justified by the fact that the probe is immersed during fluidization of the sample.

[16] Notice that when L is of the order R_e or less, a supplementary term due to the bottom of the probe has to be included. We also expected the limitation R_e to be much larger than the diameter d_g of the particles.

[17] M. E. Cates, J. P. Wittmer, J.-P. Bouchaud, and P. Claudin, Phys. Rev. Lett. **81**, 1841 (1998).

[18] L. H. Shapiro, J. B. Johnson, M. Sturm, and G. L. Blaisdell, Cold Regions Research and Engineering Laboratory Report No. 97-3, 1997 (unpublished).

[19] A. N. Bozhinskiy and K. S. Losev, *The Fundamental of Avalanche Science* (Eidgn. Insitut für Schnee- und Lawinenforschung, Davos, Switzerland, 1998).

[20] See, for example, G. Casassa, H. Narita, and N. Maeno, J. Appl. Phys. **69**, 3745 (1991).

[21] S. C. Colbeck, J. Appl. Phys. **84**, 4585 (1998).

[22] S. N. Coppersmith, C.-H. Liu, S. Majumdar, O. Narayan, and T. A. Witten, Phys. Rev. E **53**, 4673 (1996); C.-H. Liu *et al.*, Science **269**, 513 (1995).